

 Open access • Journal Article • DOI:10.1175/2009MWR2850.1

## Western North Pacific Typhoons with Concentric Eyewalls — [Source link](#)

[Hung-Chi Kuo](#), [Chih-Pei Chang](#), [Yi-Ting Yang](#), [Hau-Jang Jiang](#)

**Institutions:** [National Taiwan University](#), [Naval Postgraduate School](#)

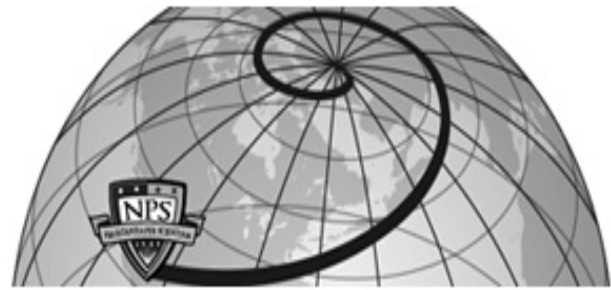
**Published on:** 01 Nov 2009 - [Monthly Weather Review](#) (American Meteorological Society)

Related papers:

- [Concentric Eye Walls, Secondary Wind Maxima, and The Evolution of the Hurricane vortex](#)
- [Hurricane Intensity and Eyewall Replacement](#)
- [Secondary eyewall formation in two idealized, full-physics modeled hurricanes](#)
- [An Objective Model for Identifying Secondary Eyewall Formation in Hurricanes](#)
- [Intensity and Structure Changes during Hurricane Eyewall Replacement Cycles](#)

Share this paper:    

View more about this paper here: <https://typeset.io/papers/western-north-pacific-typhoons-with-concentric-eyewalls-4kge0p7m9s>



**Calhoun: The NPS Institutional Archive**  
**DSpace Repository**

---

Faculty and Researchers

Faculty and Researchers' Publications

---

2009

## Western North Pacific Typhoons with Concentric Eyewalls

Kuo, H.-C.; Chang, C.-P.; Yang, Y.-T.; Jiang, H.-J.

---

Kuo, H.-C., C.-P. Chang, Y.-T. Yang and H.-J. Jiang, 2009: Western North Pacific Typhoons with Concentric Eyewalls. *Mon. Wea. Rev.* 137, 3758-3770.  
<http://hdl.handle.net/10945/36680>

---

This publication is a work of the U.S. Government as defined in Title 17, United States Code, Section 101. Copyright protection is not available for this work in the United States.

*Downloaded from NPS Archive: Calhoun*



Calhoun is the Naval Postgraduate School's public access digital repository for research materials and institutional publications created by the NPS community. Calhoun is named for Professor of Mathematics Guy K. Calhoun, NPS's first appointed -- and published -- scholarly author.

**Dudley Knox Library / Naval Postgraduate School**  
**411 Dyer Road / 1 University Circle**  
**Monterey, California USA 93943**

<http://www.nps.edu/library>

# **Western North Pacific Typhoons with Concentric Eyewalls**

**Hung-Chi Kuo**

*Department of Atmospheric Sciences, National Taiwan University,  
Taipei, Taiwan, Republic of China*

**Chih-Pei Chang**

*Department of Meteorology, Naval Postgraduate School  
Monterey, California*

**Yi-Ting Yang**

**Hau-Jang Jiang**

*Department of Atmospheric Sciences, National Taiwan University  
Taipei, Taiwan, Republic of China*

*Monthly Weather Review*

Revised February 28, 2009

Corresponding Author: Prof. Hung-Chi Kuo, Department of Atmospheric Sciences,  
National Taiwan University. No. 1, Sec. 4, Roosevelt Road, Taipei, 10617 Taiwan,  
Republic of China. E-mail: [kuo@as.ntu.edu.tw](mailto:kuo@as.ntu.edu.tw)

## ABSTRACT

This study examines the intensity change and moat dynamics of typhoons with concentric eyewalls using passive microwave data and best track data in the western North Pacific between 1997 and 2006. Of the 225 typhoons examined, we have identified 55 typhoons and 62 cases with concentric eyewalls. The data indicate that approximately 50% of Category 4 and 75% of Category 5 typhoons possessed concentric eyewalls at some point during their life time. While major typhoons are most likely to form the concentric eyewalls, the formation of concentric structure may not be necessarily at the lifetime maximum intensity. Approximately one-third of concentric eyewall cases are formed at the time of maximum intensity

A theoretical parameter called filamentation moat width is devised. The filamentation moat width can be computed from the best track typhoon intensity and the passive microwave satellite-estimated inner eyewall radius for each typhoon with concentric eyewalls. The filamentation moat width explains 40% of the variance of the satellite observed moat width in the group with concentric eyewall formation intensity greater than 130 kts. The moat is generally recognized to be heavily influenced by the subsidence forced by the two eyewalls. Our results suggest that the rapid filamentation dynamics may also be contributing to the organizational aspect of the moat in very intense typhoons.

The intensity time series in both the concentric and non-concentric composites are studied. Intensity of the concentric typhoons tends to peak at the time of secondary eyewall formation; but the standard model of intensification followed by weakening is valid for only half of the cases. Approximately 74% of the cases intensify 24 h before secondary eyewall formation and approximately 72% of the cases weaken 24 h after formation. The concentric composites have a much slower

intensification rate 12 h before the peak intensity (time of concentric formation) than that of the non-concentric composites. For Categories 4 and 5, the peak intensity of the concentric typhoons is comparable to that of the non-concentric typhoons.

However, 60 h before reaching the peak the concentric composites are 25% more intense than the non-concentric composites. So a key feature of concentric eyewall formation appears to be the maintenance of a relatively high intensity for a longer duration, rather than a rapid intensification process that can reach a higher intensity.

## 1. Introduction

Tropical cyclones (TCs), and particular strong TCs are observed with a concentric eyewall (CE) structure that has an inner eyewall and an outer eyewall separated by a convective minimum region. The secondary eyewalls are generally identified as quasi-circular rings of convective cloud. The outer eyewalls are often, but not always, collocated with the secondary wind maximum (Samsury and Zipser 1995), analogous to the collocation of the peak winds and the primary eyewall convection. Eyewall replacement cycles in such typhoons are very important for accurate forecasts of rapid intensity change (Black and Willoughby 1992). Maclay et al. (2008) identify secondary eyewall formation and eyewall replacement cycles as an internally dominant process that is responsible for structure change and thus the low-level area-integrated kinetic energy. In the past decade, the availability of satellite passive microwave data has made it possible to reveal the CE structure in TCs that had previously been difficult with only visible and infrared images. From a study of passive microwave data taken between 1997 and 2002, Hawkins and Helveston (2004) concluded that CE structure exist in a much higher percentage of TCs than had previously been estimated using visible and infrared satellite sensors. Although based on a relatively small sample, their results suggest that approximately 40% of the Atlantic, 60% of the eastern Pacific, and 80% of the western Pacific intense storms (maximum wind  $> 120$  knots  $\sim 62 \text{ m s}^{-1}$ ) have CE structures. The preponderance of large-radius CE in the western Pacific compared to other basins was further suggested by Hawkins et al. (2006). Kuo et al. (2008) discussed on the role vorticity skirts outside the TC core may play in the formation of CE structure of various sizes through the binary vortex interaction mechanism. Kossin and Sitkowski (2008) designed a new empirical model that will provide forecasters with a probability of

imminent CE formation. They identified the CE structure through a subjective visual analysis of passive microwave satellite images from the Naval Research Laboratory in Monterey covering the period of 1997-2006. In their paper, CE climatology for the North Atlantic and the central and eastern North Pacific are given. Their results of CE percentage in the Atlantic and Eastern Pacific are in general agreement with that of Hawkins et al. (2004).

The formation of the moat - the space between the inner and outer eyewalls - is a key feature for the concentric eyewalls (e.g., Houze et al. 2007). The presence of subsidence in the moat region has been demonstrated by the observational work (e.g. Dodge et al. 1999). Houze et al. (2007) have presented with aircraft observations that illustrated how the temperature and moisture profiles in the moat can evolve into a vertical structure closely resembling that found in the eye. It is generally recognized that the moat formation mechanism is heavily influenced by the subsidence forced by the two eyewalls (Dodge et al. 1999). On the other hand, Rozoff et al. (2006) proposed the idea of a rapid filamentation zone outside the radius of maximum wind of TCs. The rapid filamentation zone is a region of strain-dominated flow where the filamentation time is smaller than the 30-min moist convective overturning time. Deep convection in the rapid filamentation zone may become highly distorted and even suppressed, leading to the moat formation. Wang (2008) has found in the modeling work that the rapid filamentation process can effectively suppress high-azimuthal wavenumber asymmetries immediately outside the radius of maximum wind but has little effect on well-organized low wavenumber spiral bands. He argued that the rapid filamentation may play a secondary role in the formation of the moat in TCs. When a TC becomes very strong, it is possible that the subsidence more likely to be confined to the edge of the deep convection and strengthened by inertial stability (e.g. Rozoff et al. 2008). With a moat region of sufficient size, the

impact of subsidence may not be uniform throughout the moat and leaves the possibility that the rapid filamentation dynamics may be contributing to the organizational aspect of the moat. This maybe likely to happen in the western North Pacific due to the presence of very intense typhoons and large-radius CE cases (Hawkins et al. 2006).

This study, using passive satellite microwave and best track data sets, examines the intensity change and the moat rapid filamentation dynamics of western North Pacific CE typhoons between 1997 and 2006. Section 2 describes the data, the analysis method, and the climatology. The results regarding the relationship between moat size and filamentation dynamics are discussed in section 3, and those related to the intensity change issues are discussed in section 4. Section 5 is a summary.

## **2. Data, method and climatology**

We used the best-track data set from the Joint Typhoon Warning Center (JTWC) and microwave image sequences to examine the characteristics of typhoons with CE in the western North Pacific in the period of 1997-2006. The microwave data is the passive SSMI 85 GHz horizontal polarized orbital images obtained from the Naval Research Laboratory (NRL) Marine Meteorology Division in Monterey, CA (Hawkins et al. 2001). The NRL web site also provides the passive TRMM Microwave Imager (TMI) data from the polar orbiting TRMM satellite (Kummerow et al. 1998). The coverage of the TMI data in general is smaller than the SSMI data and yet the TMI data resolution is higher than the SSMI data. The best track data from JTWC utilizes the Geostationary Meteorological Satellite (GMS) infrared and visible cloud images as the data source for the Dvorak technique to estimate intensity. The maximum 1-min sustained wind speed was derived using the Dvorak T number.



There appears to be no formal objective definition of CE event from microwave satellite. A quasi-circular outer ring of convection that is clearly separated from the primary eyewall would visually define CE case. Our method is based on the outer eyewall deep convection (with a total blackbody temperature  $T_{bb}$  approximately 230 K) that covers 2/3 of a circle. The same criterion is applied to the satellite data with partial coverage of the passive microwave satellite data. Thus, it is possible that we missed some CE typhoons due to the partial microwave satellite coverage. The critical issues in the CE identification are the values of  $T_{bb}$  in the deep convection and the symmetry of the outer eyewalls. If we choose a  $T_{bb}$  of higher value around 235 to 240 K, we could easily double our CE cases. On the other hand, if we choose a more strict outer eyewall convection  $T_{bb}$  around 225 K, we can have just half as many of the cases as compared to that with  $T_{bb}$  230K. The results presented in the paper are more on the conservative side of evaluation that the CE structure is distinct while not too strict a definition for the outer eyewalls deep convection to retain enough cases for the statistics. The method is in general agreement with Hawkins et al. (2001) in defining the CE cases. Figure 1 gives examples of marginal accepted and rejected CE typhoon cases. There were 243 typhoons in the western North Pacific during 1997-2006, of which 18 cases were removed for missing microwave coverage for more than 24 h. A total of 55 typhoons and 62 cases were identified to possess CE structure.

The microwave data are used to define the CE structure, the inner eyewall radius, moat width, and the CE formation time. The moat is the high brightness temperature region between the eyewalls. The eyewall radius and the moat width are determined by averaging the measured values from 8 radial arms. Limited experiments with a 16-radial-arm average were found to yield similar results. The best track data provide the typhoon intensity, intensity change, location, and lifetime maximum

intensity. The JTWC best track is in 6 h time resolution. We account for the irregular satellite observation times with the regular JTWC best track data by matching the time closest to the satellite observation. These data are used to compute the CE formation percentage and analyze the relationships between moat and intensity, CE, and intensity change, and compare the intensity changes of concentric typhoons with the non-concentric typhoons. Note that the two data sets used are not totally independent as JTWC considered the microwave imageries (such as SSM/I and TMI) in producing the best track data. While the data are not totally independent of each other, using them together is still the only way to provide a quantitative estimate of the formation percentages and their distribution relative to intensity.

Figure 2 gives the locations of CE formation events in the western North Pacific between 1997 and 2006. The seasonal cycle of CE formation is represented by green (April, May, and June), red (July, August, and September), and blue (October, November, and December) colors. The dots display the locations of typhoons with intensity greater than or equal to Category 4 on the Saffir-Simpson scale. The circles indicate the locations of CE formation. A dot inside a circle indicates CE formation with intensity greater than or equal to Category 4. Figure 2 suggests that strong typhoons containing CE structure tend to occur further west in the basin. This may be due to the fact that typhoons tend to be stronger in west of the basin after a long journey over ocean. Figure 3 gives the number and the average latitude of CE formation by month. The black, gray and white bars represent the number of CE cases in Category 5, Category 4, and less than Category 4 intensities. The upper (lower) curve indicates the average latitude typhoon concentric eyewall formation with intensity less than Category 4 (greater or equal to Category 4) by month. The percentages by month on top of the diagrams are the ratio of CE cases with intensity greater than or equal to Category 4. The majority of typhoons with CE structure (54

cases out of the total 62 cases) form between June and October. While fewer cases are found during November, December, April, and May, most of the CE cases (41 cases out of the total 62 cases) are found with formation intensity at Categories 4 and 5. Figures 2 and 3 indicate a northern seasonal migration of CE structure formation locations. Between June and October, the weaker intensity cases are located at higher latitudes than the stronger intensity cases. Both the internal and external dynamics may play important role in CE formations. Examples of internal dynamics are the propagating vortex Rossby waves interact with critical radius (Montgomery and Kallenbach 1997) and axisymmetrization of binary vortex interaction (Kuo et al. 2004, 2008). These dynamics highlight the importance of the strong core vortex. On the other hand, Nong and Emanuel (2003) showed that the CE may form due to some favorable ambient environment conditions or external forcing and WISHE instability. It is possible that external forcings may be important for this high latitude CE with weaker formation intensity.

Figure 4a shows a histogram of the CE cases for each typhoon intensity category according to the Saffir-Simpson scale. Of the 225 typhoons examined, we identify approximately one quarter of typhoons possessed the CE structure. Of the 55 typhoons with CE structure, 83% or 47 typhoons reached Categories 4 and 5. Specifically, the data indicate that 57% of Category 4 and 72% of Category 5 typhoons possessed CE structure at some point during their lifetime. This result agrees with the general notion that CE structures are associated with TCs of sufficient strength. The results are also in general agreement with the North Atlantic climatology of Kossin and Sitkowski (2008). Kossin and Sitkowski (2008) found that one-third of all hurricanes developed a CE structure at least once during their life time. Comparatively, 70% of major hurricanes (Category 3-5) were observed to form CE structures at least once in their lifetime. They also show that the hurricane is

apparently more likely to form a CE structure in July or September than other month.

Figure 4b is similar to Fig. 4a except the horizontal coordinate is the intensity at the time of secondary eyewall formation rather than the maximum intensity of each typhoon. Secondary eyewalls were observed to form within a broad range of intensities. Due to the inclusion of the seven multiple concentric formation cases, the total CE case numbers in Fig. 4b is 62 rather than the 55 in Fig. 4a. Figure 4b indicates that 66% of the CE cases formed at Category 4 and 5 strengths; the percentage is lower than what is indicated in Fig. 4a. This implies that while CE structure often form in typhoons of sufficient strength, they may not necessarily form when the typhoons are at their peak intensity. An analysis of the time of concentric eyewall formation relative to the time of lifetime maximum intensity is given in section 4.

### 3. Moat size and filamentation dynamics

Figure 5 shows four scatter diagrams involving the moat width ( $d_0$ ), the cyclone core size in terms of inner eye radius ( $r_0$ ), and the cyclone intensity at CE structure formation ( $V_m$ ). Figure 5a is moat width versus core size, Fig. 5b is core size versus cyclone intensity, Fig. 5c is moat width versus estimated cyclone core vorticity strength ( $\zeta_0 = 2V_m/r_0$ , with the solid body rotation assumption) and Fig 5d is moat width versus cyclone intensity. The green, black, and red circles indicate categories 3, 4, and 5, respectively. The filled circles are the averaged values for the respective categories. In general, the large scatters in these figures indicate no significant relationship between the moat width, core size, core vorticity, and intensity for the concentric eyewall typhoon cases. This lack of relationship between the kinematic parameters seems to imply that dynamic processes are not solely responsible for moat formation.

The presence of subsidence in the moat region has been demonstrated by the observational work (e.g. Dodge et al. 1999). Houze et al. (2007) have presented observations that illustrated how the temperature and moisture profiles in the moat can evolve into a vertical structure closely resembling that found in the eye. These observations underline the important role of subsidence in moat formation physics. Rozoff et al. (2006) called attention to the idea of a rapid filamentation zone outside the radius of maximum wind in strong tropical cyclones. The rapid filamentation zone is a region of strain-dominated flow where the filamentation time is shorter than the typical moist convective overturning time. Without adequate time for organization, deep convection in the rapid filamentation zone may become highly distorted and even suppressed, leading to the formation of a moat. The strain effect associated with the vortex most likely decreases the probability of secondary eyewall formation within a certain radial distance of the primary eyewall, thus becoming a factor in determining the moat width.

In order to evaluate the role that rapid filamentation dynamics may play in the moat formation mechanism, we will compare the moat width predicted by the rapid filamentation dynamics to that observed from the microwave satellite data. Mallen et al.'s (2005) aircraft flight-level data analysis shows that TCs are often characterized by a relatively slow decrease of tangential wind outside the radius of maximum wind, and hence by a corresponding cyclonic vorticity skirt. We will assume that the vortex is in solid body rotation inside the radius of maximum wind and the tangential wind decreases according to  $r^{-\alpha}$  outside of the radius of maximum wind, where  $\alpha$  is the skirt parameter.

Starting with the best track intensity  $V_m$  and satellite estimated core size  $r_0$ , the core vorticity strength is  $\zeta_0 = 2V_m/r_0$ , and the total strain rate in terms of the

vorticity is  $S_1^2 + S_2^2 = [(1 + \alpha)/2]^2 \zeta_0^2 (r_0/r)^{2+2\alpha}$ . The filamentation time based on Rozoff et al. (2006) is  $\tau_{fil} = 2(S_1^2 + S_2^2 - \zeta^2)^{-1/2}$  for  $S_1^2 + S_2^2 > \zeta^2$ .  $\zeta$  is the vorticity at the moat. Thus,  $S_1^2 + S_2^2 - \zeta^2 = \alpha \zeta_0^2 (r_0/r)^{2+2\alpha}$ , and the filamentation time is  $\tau_{fil} = 2/(\sqrt{\alpha} \zeta_0) (r/r_0)^{1+\alpha}$ . We then define the convective overturning time  $\tau_{con} = 30$  mins, the time for a parcel traveling from the top of the boundary layer (600m) to cloud top (15 km) with a typical speed  $8 \text{ m s}^{-1}$ , or for a weaker updraft of  $3\text{-}4 \text{ m s}^{-1}$  that extends slightly above freezing level before merging into a region of general mesoscale lift. We then define the rapid filamentation zone as a region where the filamentation time is smaller than the convective overturning time.

$\tau_{con} = 2/(\sqrt{\alpha} \zeta_0) (r^*/r_0)^{1+\alpha}$ , and  $r^* = (\sqrt{\alpha} \zeta_0 \tau_{con}/2)^{1/(1+\alpha)} r_0$ . The width of the rapid filamentation zone is  $d_{\hat{r}} = r^* - r_0 = \left[ (\sqrt{\alpha} \zeta_0 \tau_{con}/2)^{1/(1+\alpha)} - 1 \right] r_0$ .

In summary, the rapid filamentation zone is a function of the convective overturning time, the vorticity determined from the best track intensity, satellite estimated core size, and the skirt parameter.

Figure 6 gives the variance explained by the non-dimensional moat width to that of the observed non-dimensional moat width. The non-dimensional width calculation is according to the core size  $r_0$  in each CE typhoon. Figure 6a gives the moat width variance explained for the CE typhoons when their formation intensity is greater (smaller than and equal to) than some intensities ranging downward from 135 kts in every 5 kts. The skirt parameters used in the calculations are 1, 0.5, and 0.3. The 0.3 value is corresponding to a situation of very slow decay of tangential wind outside the core. Figure 6a suggests that, regardless the skirt values used, the filamentation moat width explains 40% of the variance of the satellite observed moat width in the group with CE formation intensity greater than 130 kts (19 cases). We have performed test

by randomly assign different skirt parameter values to these 19 cases and still yield the similar 0.4  $R^2$  values. The scatter plot and the variance explained for CE formation intensity of Category 5, 4, and 3 ( $\alpha=0.5$ ) are shown in the Figure 6b, 6c, and 6d respectively.

Figure 6 suggest that the filamentation dynamics appear to be important in the group with the strongest CE formation intensity. Rozoff et al. (2008) showed that the subsidence in the moat may become most important in the later stages of CE formation. The strengthening convection in the outer eyewall may lead to enhanced up-down circulation and inertial stability, which in turns leads to the narrowing (or confinement ) of up-down circulation that enhances the local subsidence. When the strong subsidence is confined by inertial stability to the edge of the deep convection for a very strong TC, the impact of subsidence may not be uniform in the moat region if the moat is of the sufficient size. This leaves the possibility that rapid filamentation in strong CE typhoons may be contributing to the organizational aspect of the moat in the early stage. This maybe likely to happen in the western North Pacific due to the prevalence of large-radius CE cases (Hawkins et al. 2006; Kuo et al. 2008).

#### **4. Intensity change**

The evolution of intensity surrounding CE formation is analyzed by compositing with respect to the CE structure formation time. The composite time series of intensity is further classified into PN, PP, NP, and NN four groups. The classification is according to the 24 h intensity change before and after the formation. Here the letter N indicates negative intensity trend and the letter P indicates positive intensity trend. The first letter in each group's name indicates the intensity change in the last 24 h prior to formation and the second letter the intensity change during the first 24 h after the formation. For example, the NP group showed weakening prior to formation and

strengthening after the CE formation, all within 24 h of the formation time. We will not classify the CE cases in the above group if the typhoon center is somewhere 200 km near the land prior to or after 24 h CE formation. We hope to exclude the land intensity weakening effect from our intensity change study.

While the major typhoons are likely form CE structure, Fig. 4 indicates that the CE structure may not necessarily form when the typhoons are at their peak intensity. Figure 7 is an analysis of the CE formation time relative to the time of lifetime maximum intensity. There are approximately 1/3 of CE cases (20 cases) which are formed at the time of maximum intensity and slightly less than 1/4 of the cases (15 cases) formed within time interval 30 h after typhoon lifetime maximum intensity. There are 23 out of 62 cases CE formation time is greater than 30 h after the maximum intensity time. Of these cases, there are 6 multiple CE formation cases; and 11 cases are formed within 24 hr of the typhoon second intensity peak time. There are thus half of the cases (31 cases of PN group) has peak intensity at the CE formation time.

Figure 8 gives the composite time series of intensity as well as the percentage of NP, NN, PN, and PP cases. The standard deviation in these composite is on the order of 15 kts. More than half (51%) of the CE formation cases are in the PN group in which the intensity increases 24 hours before the CE formation and followed by a weakening in the next 24 h. It is noted that 19 of the 24 typhoons in this group are of Category 4 and 5 CE forming intensity. The averaged composite and the PN group agree with the typical notion that the CE structure often forms in stronger tropical cyclones and those tropical cyclones often weaken after a secondary eyewall forms.

Besides the PN group, most of the CE cases are in the PP and NN groups. The PP (NN) group possesses 12 (11) CE cases and NP group has only 2 cases. Figure 8 indicates that the intensity increase after the CE formation in the NP and PP groups is



not as significant as that prior the CE formation. It is more appropriate to read the second P in our stratification as the typhoons maintain its intensity in the 24 h after the CE formation. Note that the PP group has a mean CE forming intensity approximately  $10 \text{ ms}^{-1}$  stronger than that in the NN group. The NP group has the weakest CE forming intensity. There are 7 out of 12 typhoons in the PP group possess the Categories 4 and 5 CE forming intensity. On the other hand, 9 out of the 13 typhoons in the NN and NP groups have CE formation intensity at Categories 2 and 3. The majority of typhoons in the NN and NP groups may not have peak intensity at their CE formation time. Overall, while only half of the cases peak at the time of CE formation, approximately 73% of the cases intensify 24 h before CE formation and approximately 71% of the cases weaken 24 h after CE formation.

An example of the structure from each of the four groups is given in Figure 9 by displaying the color-enhanced microwave images before, at, and after concentric eyewall formation and the corresponding intensity time series. The time difference between the CE formation time and time of maximum intensity is also shown. The microwave imagery in the PN case agrees with the typical eyewall replacement cycle model (e.g. Black and Willoughby 1992), in which the inner eyewall dissipates after the secondary eyewall forms, and the intensity decreases. However, the PP, NN, and NP cases do not fit this model. We have examined the sea surface temperature and vertical wind shear of these groups as compared to those in the PN group and could not find a definite difference. It seems that the intensity change in these groups may be related to the CE dynamics. For example, the intensity in the PP case of Typhoon Amber (1997) appears to be increasing from 24 h before to 24 h after the formation of the CE structure. The microwave imagery also indicates that the CE structure was maintained for at least of 24 h after formation, with no eyewall replacement cycle observed. The NN and NP cases often show a larger moat size (NN 45 km in 11 cases

averaged and NP 50 km in 2 cases averaged) and still identifiable inner eyewall for a period of 24 h.

We compare the intensity change in the CE cases with that of non-concentric cases in Fig. 10. For the concentric time series the composites were done relative to the time of CE formation while for the non-concentric cases they were done relative to the peak intensity time. Figure 10 also gives the normalized intensity change. The normalization for the non-concentric cases is with their life time peak intensity and the normalization for the concentric cases is with their intensity at time of CE formation. Figure 10a and 10b are for stronger typhoon (Categories 4 and 5) formation cases and the Fig. 10c and 10d are for weaker typhoons (Categories 2 and 3), with the left panels showing the intensity changes and the right panels the normalized intensity changes. The “total” curve in Fig. 10 is the composite for all typhoon cases except Category 1.

Figure 10 shows that the composite intensity tendency for all CE typhoons prior to formation is distinctively different from the non-concentric typhoons prior to reaching maximum intensity. The concentric composite reaches a higher normalized intensity prior to formation than the non-concentric composite prior to peak intensity. However, the intensity tendencies for both strong concentric and non-concentric typhoons are similar in the weakening phase. There is also some difference between the strong (Categories 4 and 5) and weak (Categories. 2 and 3) CE typhoons, in that the former undergo a period of sustained intensification while the latter more or less just maintain their intensity with only modest intensification. The weakening tendencies in the weak cases of CE formation however, are slower than in the strong cases. Compared to the non-concentric eyewall cases, the formation of concentric eyewalls depends on the maintenance of a relatively high intensity for a longer duration prior to formation, rather than a rapid intensification process that can reach a

higher intensity.

Figure 11 shows composite time series of the normalized intensity for the concentric and non-concentric cases in the western North Pacific in addition to the normalized intensity associated with the average tropical cyclones in the Atlantic and western North Pacific that did not encounter cold water or make landfall as reported by Emanuel (2000), and annular hurricanes reported by Knaff and Kossin (2003). In our results, the cases near landfall were excluded. The intensity tendencies of our non-concentric cases are in general agreement with Emanuel (2000). Compared to the non-concentric eyewall typhoon composite, the concentric composite shows a relatively high intensity for a longer duration, rather than a rapid intensification process that can reach a higher intensity. Kuo et al. (2004, 2008) hypothesized that axisymmetrization of positive vorticity perturbations around a strong and tight core of vorticity may lead to the formation of concentric eyewalls. The long duration of high intensity before secondary eyewall formation may provide a favorable environment for the axisymmetrization dynamics to operate.

## **5. Summary**

Using the best track data and passive microwave satellite imagery we studied western North Pacific typhoons with CE structure during 1997-2006. Our results are:

- (1) Most of the CE cases occur between June and October. There is a northern seasonal migration of CE formation locations. The CE structures formed at a weaker intensity are often located at higher latitude.
- (2) Approximately one quarter of the cases examined possessed CE structure; including 50% of Category 4 and 75% of Category 5 typhoons possessed CE at some point during their life time. Approximately one-third of CE cases are formed at the time of maximum intensity and a quarter of the CE cases are formed within

- 30 h after the time of maximum intensity.
- (3) There is no significant relationship between core size, intensity, core vorticity, and moat width for typhoons with CE typhoons.
  - (4) A theoretical filamentation moat width is calculated based on the observation data and comparing it with the satellite-estimated moat width. The filamentation moat width explains 40% of the variance of the satellite observed moat width in the group with CE formation intensity greater than 130 kts. The results appear to suggest that the rapid filamentation dynamics may also be contributing to the organizational aspect of the moat in very strong typhoons.
  - (5) Intensity of the CE typhoons tends to peak at the time of secondary eyewall formation but the standard model of intensification followed by weakening is valid for only half of the cases. Approximately 74% of the cases intensify 24 h before secondary eyewall formation and approximately 72% of the cases weaken 24 h after formation.
  - (6) A major difference between the concentric cases and non-concentric cases is the intensity and intensity change during the pre-formation or intensification stage. The concentric cases are marked by a relatively high intensity lasting for a longer duration prior to formation, rather than a rapid intensification process that can reach a higher intensity as is for most non-concentric cases.
  - (7) There is no significant difference in the decaying rate of intensity for both concentric and non-concentric cases after formation or reaching peak intensity.

### *Acknowledgement*

We wish to thank Jeffrey Hawkins and reviewers for helpful comments and suggestions. The satellite microwave images were made available by the Naval Research Laboratory Marine Meteorology Division in Monterey, California. This research was supported by Taiwan's National Research Council through grants NSC96-2111-M-002-002, NSC95-2745-P-002-004, and MOTC-CWB-96-2M-01 to National Taiwan University, and by the US Office of Naval Research to Naval Postgraduate School.

## References

- Black, M. L., and H. E. Willoughby, 1992: The concentric eyewall cycle of Hurricane Gilbert. *Mon. Wea. Rev.*, **120**, 947-957.
- Dodge, P., R. W. Burpee, and F. D. Marks Jr., 1999: The kinematic structure of a hurricane with sea level pressure less than 900 mb. *Mon. Wea. Rev.*, **127**, 987-1004.
- Emanuel, K., 2000: A statistical analysis of tropical cyclone intensity. *Mon. Wea. Rev.*, **128**, 1139-1152.
- Hawkins, J. D., T. F. Lee, F. J. Turk, C. Sampson, J. Kent, and K. Richardson, 2001: Real-time internet distribution of satellite products for tropical cyclone reconnaissance. *Bull. Am. Meteorol. Soc.*, **82**, 567-578.
- Hawkins, J. D., and M. Helveston, 2004: Tropical cyclone multiple eyewall characteristics. Preprints, 26<sup>th</sup> Conference on Hurricane and Tropical Meteorology, Miami, FL., *Amer. Meteor. Soc.*, 276-277.
- Hawkins, J. D., and M. Helveston, T. F. Lee, F. J. Turk, K. Richardson, C. Sampson, J. Kent, and R. Wade, 2006: Tropical cyclone multiple eyewall characteristics. Preprints, 27<sup>th</sup> Conference on Hurricane and Tropical Meteorology, Monterey, CA, *Amer. Meteor. Soc.*
- Houze, R. A., S.-S. Chen, B. F. Smull, W.-C. Lee and M. M. Bell, 2007: Hurricane intensity and eyewall replacement. *Science*, **315**, 1235-1239.
- Knaff, J. A., and J. P. Kossin, 2003: Annular Hurricanes. *Wea. Forecasting*, **18**, 204-223.
- Kossin, J. P., and M. Sitkowski, 2008: An objective model for indentifying secondary eyewall formation in hurricanes. *Mon. Wea. Rev.*, accepted.
- Kummerow, C., W. Barnes, T. Kozu, J. Shiue, and J. Simpson, 1998: The Tropical Rainfall Measuring Mission (TRMM) sensor package. *J. Atmos. Oceanic*

*Technol.*, 15, 809-817.

- Kuo, H.-C., L.-Y. Lin, C.-P. Chang, and R. T. Williams, 2004: The formation of concentric vorticity structures in typhoons. *J. Atmos. Sci.*, **61**, 2722-2734.
- Kuo, H.-C., W. H. Schubert, C.-L. Tsai, and Y.-F. Kuo, 2008: Vortex interactions and barotropic aspects of concentric eyewall formation. *Mon. Wea. Rev.*, **136**, 5183-5198.
- Mallen, K. J., M. T. Montgomery, and B. Wang, 2005: Reexamining the near-core radial structure of the tropical cyclone primary circulation: Implications for vortex resiliency. *J. Atmos. Sci.*, **62**, 408--425.
- Maclay, K. S., M DeMaria, and T. H. Vonder Haar, 2008: Tropical cyclone inner-core kinetic energy evolution. *Mon. Wea. Rev.*, Accepted.
- Rozoff, M. C., W. H. Schubert, B. D. McNoldy, and J. P. Kossin, 2006: Rapid filamentation zones in intense tropical cyclones. *J. Atmos. Sci.*, **63**, 325-340.
- Rozoff, M. C., W. D. Tervey W. D., M. T. Montgomery, and W. H. Schubert, 2008: The response of deep convective clouds to tropical cyclone-like horizontal and vertical shears. Submitted to *J. Atmos. Sci.*
- Rozoff C. M., W. H. Schubert, and J. Kossin, 2008: Some dynamical aspects of tropical cyclone concentric eyewalls. *Q. J. R. Meteorol. Soc.*, Accepted.

## Figure Captions

Figure 1. Color-enhanced microwave images of Typhoon Yagi and Typhoon Saomai. Typhoon Yagi is identified as concentric case while Typhoon Saomai is classified as no concentric case. Saomai maximum intensity is 140 kts at 0809-1200Z.

Figure 2. Locations of concentric eyewall formation events in the western North Pacific between 1997 and 2006. The seasonal cycle of concentric eyewall cases is represented by green (April, May, and June), red (July, August, and September), and blue (October, November, and December) colors. The dots display the locations of typhoons with intensity greater than or equal to Category 4 on the Saffir-Simpson scale. The circles indicate the locations of concentric eyewall formation. A dot inside a circle indicates concentric eyewall formation with intensity greater than or equal to Category 4.

Figure 3. The number and the average latitude of concentric eyewall formation by month. The black, gray, and white bars represent the number of concentric eyewall cases of Category 5, Category 4, and less than Category 4 intensity. The upper (lower) curve with circle (a dot inside the circle) indicates the average latitude of concentric eyewall formation with intensity less than Category 4 (greater than or equal to Category 4) by month. The percentages by month on top of the diagrams are the percentage of concentric eyewall typhoons with intensity greater than or equal to Category 4.

Figure 4. (a) Histogram of the concentric cases against the typhoon intensity as categorized by the Saffir-Simpson scale. (b) As in Fig. 3a except against the typhoon



intensity at the time of secondary eyewall formation.

Figure 5. (a) Scatter diagram of moat width versus of cyclone core size. (b) cyclone core size versus cyclone intensity .(c) moat width versus estimated cyclone core vorticity strength.(d) moat width versus cyclone intensity for the concentric eyewall cases studied. The red, black and green circles respectively indicate .The cyclone core size and the moat width are determined from microwave data and the intensity from the best track data. The cyclone core vorticity is estimated from the core size and the intensity. Note the wide scatter of values.

Figure 6. (a) Scatter diagram of R2 versus cyclone intensity. The circles (squares ) indicate R2 which is the relationship between non-dimensional moat width and non-dimensional filamentation moat width for concentric cases intensity greater than(smaller than and equal to) different intensity. The black, deep gray and light gray colors display  $\alpha=0.3$ ,  $\alpha=0.5$  and  $\alpha=1$ , respectively. (b) Scatter diagram of non-dimensional moat width versus of the non-dimensional filamentation moat width for concentric cases in Category 5. The vortex structure is assumed with the skirt parameter of 0.5. (c) Same as Fig. 5b except concentric cases in Category 4(d) Same as Fig. 5b except concentric cases in Category 3.

Figure 7. (a) The concentric forming intensity and the difference between the formation time and the maximum intensity time (0 h). The triangles indicate cases that prior to or after 24 h concentric eyewall formation, the cyclone center about 200 km near the land. The circles display the no land influence cases. (b) Histogram of the concentric cases against the difference between the concentric eyewall formation time and the maximum intensity time in PN, PP, NN, NP, and Land cases.

Figure 8. Composite time series of the intensity for NP, NN, PN, and PP cases. The composite was done with respect to the secondary eyewall formation time. The percentage of each case is also shown. The first letter N (P) represents that the intensity decreases (increases) 24 hours before the concentric eyewall formation. The second letter N (P) represents that the intensity decreases (increases) 24 hours after the concentric eyewall formation. More than half of the concentric eyewall formation cases are in the PN case, where the intensity increases (decreases) before (after) the concentric eyewall formation.

Figure 9. Color-enhanced microwave images before, at, and after concentric eyewall formation for typical PN, PP, NN, and NP cases. The corresponding intensity time series is also shown. The length scale of  $2\sigma$  in the satellite picture is indicated. The numbers in time series of intensity display the difference between the concentric eyewall formation time and the maximum intensity time.

Figure 10. Composite time series of intensity for the concentric and non-concentric cases. Compositing was done relative to the time of concentric eyewall formation (maximum intensity) for the concentric typhoon cases (non-concentric typhoon cases). (a) and (b) is the composite time series of intensity and normalized intensity respectively for Category 4 and 5 typhoons. (c) and (d) are the similar composites except for Category 2 and 3 typhoons. The “total” curves are the composites of concentric cases in all categories.

Figure 11. Composite time series of the normalized intensity for the concentric and non-concentric cases in the western North Pacific. Also plotted are the normalized intensity associated with average tropical cyclones in the Atlantic and western North

Pacific that did not encounter cold water or make landfall as reported by Emanuel (2000) and annular hurricanes as reported by Knaff et al. (2003). Compositing was done relative to the time of concentric eyewall formation (maximum intensity) for the concentric (non-concentric cases) .